

DESIGN OF Ag-Ge-Zn BRAZE/SOLDER ALLOYS: EXPERIMENTAL THERMODYNAMICS AND SURFACE PROPERTIES

S. Delsante ^{a,b}, D. Li ^a, R. Novakovic ^b, G. Borzone ^{a,b,*}

^a Department of Chemistry and Industrial Chemistry, Genoa University and Genoa Research Unit of INSTM, Genoa, Italy

^b Institute of Condensed Matter Chemistry and Energy Technologies, National Research Council (ICMATE-CNR), Genoa, Italy

(Received 26 June 2017; accepted 20 September 2017)

Abstract

The experimental investigation of the Ag-Ge-Zn phase diagram was performed by using combined microstructural and Differential Scanning Calorimeter (DSC) analyses. The samples were subjected to thermal cycles by a heat-flux DSC apparatus with heating and cooling rate of 0.5 or 0.3 °C/min.

The microstructure of the samples, both after annealing and after DSC analysis, was studied by optical and scanning electron microscopy coupled with EDS (Energy Dispersive Spectroscopy) analysis. Considering the slow heating and cooling rate adopted, the isothermal section at room temperature was established. No ternary compounds were observed. On the basis of the experimental investigations the invariant reactions were identified.

Combining the thermodynamic data on the Ag-Ge, Ag-Zn and Ge-Zn liquid phases by means of Butler's model the surface tension of Ag-Ge-Zn alloys was calculated.

Key words: Ag-Ge-Zn; Solder alloys; Differential scanning calorimetry; Liquidus projection; Isothermal section; Surface tension.

1. Introduction

Ag-based alloys have industrial importance in relation to their use as high temperature solders in jewellery [1]. Silver solders usually are based on the Ag-Cu binary system, nevertheless Zn can be considered a candidate for replacing copper; it reduces the melting point of solder, increases the fluidity of the alloys and deoxidizes the melt. The very good tarnish-resistance of Ag-Ge and Ag-Ge-Zn alloys [2] make them good candidates for bonding sterling silver (Ag92.5Cu7.5 wt.%) which are commonly used in jewellery for its very special lustre and very good mechanical properties. Furthermore, Ag-Ge alloys are also employed as braze for thermoelectric modules [3].

There is no literature data neither on phase diagram nor on thermodynamic properties for the Ag-Ge-Zn system. Concerning the surface properties, only data for the binary Ag-Ge subsystem are available [4,5].

The thermal behaviour and the phase relations of the Ag-Ge-Zn alloys were experimentally investigated in the present work. In addition, taking

into account the relevance of the Ag-Ge-Zn system in joining processes, the surface tension of the binary and ternary alloys were calculated using the Butler model [6,7] and compared with available literature data.

2. Literature data

The literature data on boundary binary diagrams and intermetallic phases are summarized in Tables 1 and 2.

2.1 Ag-Zn system

The equilibrium diagram of the Ag-Zn system has been established by Andrews et al. [8] and redrawn by Massalski [9]. More recently, the Ag-Zn phase diagram has been assessed by different authors [10-12]. The Ag-Zn system shows the formation of a series of intermediate phases; the names, structure types and Pearson's symbol relevant to the Ag-Ge-Zn system are reported in Table 1.

Appreciable solubility of Zn in fcc Ag (maximum solubility 40.2 at %Zn at 258 °C) and the small

* Corresponding author: gabriella.borzone@unige.it

solubility of Ag in Zn (5 at. % at 431 °C) is reported. The current accepted Ag-Zn phase diagram is characterized by four peritectic, one eutectoid and one peritectoid reactions, see Table 2.

2.2 Ag-Ge system

The binary Ag-Ge phase diagram is characterised by an eutectic reaction at 651 °C with small but appreciable solubility of Ge in fcc Ag and negligible solubility of Ag in Ge [14,15] (see Tables 1 and 2). These data are confirmed in a more recent reassessment [16]; the formation of a metastable phase with hcp structure was obtained by rapid quenching as reported in [17]. Concerning the surface tension experimental data, there are two datasets [4,5] available in literature.

2.3 Ge-Zn system

The Ge-Zn phase diagram was assessed by R.W.Olesinski and G.J.Abbaschian [18]. Negligible mutual solid solubility of germanium and zinc and an eutectic reaction at 394 °C and 94.7 at.% Zn is reported (see Table 1 and 2).

Table 1. Ag-Ge-Zn system. Crystal structures of the phases related to the binary boundary systems [9, 13].

Phase	Pearson's symbol and prototype	Phase boundary limits
(Ag)	cF4- Cu	xGe \cong 0.10 (T=651 °C), xZn = 0.402 (T=258 °C)
(Ge)	cF8-C (diamond)	xAg \approx 0, xZn \approx 0
(Zn)	hP2-Mg	xAg = 0.05 (T=431 °C), xGe \approx 0
AgZn-HT, β	cI2-W	0.367 < xZn < 0.586
AgZn-LT, ζ	hP9- AgZn	0.37 < xZn < 0.51
Ag ₅ Zn ₈ , γ	cI52- Cu ₅ Zn ₈	0.595 < xZn < 0.63
\approx AgZn ₃ , ϵ	hP2-Mg	0.678 < xZn < 0.872

To the best of our knowledge, no literature data on the phase diagram, thermodynamic and surface properties of the Ag-Ge-Zn system are available.

3. Materials and method

More than twenty Ag-Ge-Zn ternary alloys were prepared and characterised. The starting materials were Ag (Johnson-Matthey Ltd.) 99.99%, Ge (Koch Light Lab.) 99.999%, and Zn (Prolabo) 99.999

Table 2. Ag-Ge-Zn system. Invariant reactions in the binary boundary systems [9].

System	Reaction	Symbol	T/ °C
Ag-Zn (at.% Zn)	L(37.5)+(Ag) \rightleftharpoons β	p ₁	710
	L(61.8) + β \rightleftharpoons γ	p ₂	661
	L (71.0)+ γ \rightleftharpoons ϵ	p ₃	631
	L (98) + ϵ \rightleftharpoons (Zn)	p ₄	431
	β + γ (58.5) \rightleftharpoons ζ (50.4)	p ₅	274
	β (45.6) \rightleftharpoons (Ag) + ζ	e ₃	258
Ag-Ge (at.%Ge)	L(24.5) \rightleftharpoons (Ag) + (Ge)	e ₁	651
Ge-Zn (at.%Zn)	L (94.7) \rightleftharpoons (Ge) + (Zn)	e ₂	394

mass.% purity. Weighed pieces of Ag, Ge and Zn were sealed in quartz tube under Ar atmosphere. The ingots were melted in a resistance furnace (Carbolite®) equipped with a digital controller and kept at 750 °C for a variable time from 30 to 120 minutes in order to get homogeneous liquid alloys which were slowly cooled with a rate of 1 or 0.5 °C/min. One piece of around 0.5 grams from each synthesized alloy was cut and sealed in a Ta crucible under Ar atmosphere for DSC analysis. Portions of ingots of selected alloys were subjected to homogenization heat treatment, annealing at 200 °C for 50 days, followed by heating up to 250 °C, maintained at this temperature for 27 days and then slowly cooled inside the furnace to room temperature.

After DSC measurements and annealing treatments, the samples were characterized by Light Optical Microscopy (LOM), Scanning Electron Microscopy (SEM) and energy-dispersive X-ray spectroscopy (EDS) to examine microstructures, identify the phases and measure their composition on polished unetched surfaces.

Table 3 summarises the global composition of the samples measured by SEM/EDS.

DSC measurements were performed in argon gas using a Setaram DSC111 apparatus in a continuous mode, to determine the phase transition temperatures. This apparatus is designed as a Calvet calorimeter where the cylindrical reference and working cells are surrounded by two differentially connected thermal fluximeters. The temperature scale and sensitivity were checked with standard materials. Differences in fusion temperatures were found to be less than ± 1 °C. The measurements were generally conducted between 200 and 750 °C. The Ag-Ge-Zn samples were subjected to thermal cycles with a heating and cooling rates of 0.5 or 0.3 °C/min. After DSC analysis the microstructure of all samples was investigated by optical and scanning electron microscopy. A Leica



Digital Microscope and a Zeiss Evo 40 equipped with a Pentafet Link Energy Dispersive X-ray Spectroscopy (EDS) system managed by the INCA Energy software (Oxford Instruments, Analytical Ltd., Bucks, U.K.) were employed. The microscope was operated at an acceleration voltage of 20 kV and calibration for the quantitative measurements was performed by a Co standard.

Table 3. SEM/EDS global composition of the Ag-Ge-Zn alloys, primary phases upon solidification and phase transformation temperatures measured by DSC during heating (*i* = invariant reaction, *m* = monovariant, *l* = liquidus).

#	EDS global composition (at.%)			Primary phase	DSC Signal on Heating (T/ °C)		
	Ag	Ge	Zn				
1	77	11	12	(Ag)	-	624 (m)	777 (l)
2	76.5	11	12.5	(Ag)	-	624 (m)	769 (l)
3	70	20	10	(Ag)	-	624 (m)	663 (l)
4	61	24	15	(Ge)	-	616 (m)	652 (l)
5	61	11	28	(Ag)	-	606 (m)	651 (l)
6	61	14	25	(Ag)	-	607 (m)	648 (l)
7	58	18	24	(Ag)	-	607 (m)	650 (l)
8	56	16.5	27.5	(Ag)	-	606 (m)	622 (l)
9	54	31.5	14.5	(Ge)	-	610 (m)	695 (l)
10	52	16	32	(Ag)	602 (i) - U ₁ 263 (i) - U ₅	611 (m)	614 (l)
11	49	34.5	16.5	(Ge)	-	610 (m)	727 (l)
12	47	15.5	37.5	(Ge)	600 (i) - U ₁ 264 (i) - U ₅	609 (m)	618 (l)
13	42	13	45	β	592 (i) - U ₂ 281 (i) - P ₁	596 (m)	604 (l)
14	42	16	42	(Ge) Few	281 (i) - P ₁	593 (m)	610 (l)
15	39	36	25	(Ge)	600 (i) - U ₁ 263 (i) - U ₅	602 (m)	713 (l)
16	36.5	24.5	39	(Ge)	590 (i) - U ₂ 282 (i) - P ₁	597 (m)	672 (l)
17	37	14	49	γ	281 (i) - P ₁	583 (m)	593 (l)
18	32	12	56	γ	570 (i) - U ₃	576 (m)	588(l)
19	26	13.5	60.5	ε	-	560 (m)	592 (l)
20	6	4	90	ε	400 (i) - U ₄	-	504(l)

4. Modelling of surface tension

The knowledge of thermodynamic data on mixing, the shape of the corresponding mixing function curves

(i.e. the enthalpy of mixing, the Gibbs free energy of mixing and the activities) and the type of phase diagram, are necessary to select the most appropriate model to describe the surface properties of liquid alloys. The models used to describe the surface tension of liquid alloys are detailed in [19]. The aforementioned thermodynamic properties of the Ag-Ge-Zn together with its constitutional Ag-Ge, Ag-Zn and Ge-Zn binary systems characterise all the systems as weakly interacting, and to calculate the surface tension of these alloys the Butler model was applied. Details on Butler's model are reported in many contributions [6, 7, 20, 21]. It is important to mention that, for weakly interacting systems, the theoretical values obtained by Butler's model or by Quasi Chemical Approximation (QCA) for the regular solution are very close to each other and, moreover, in some cases such models predicted values which may overlap [19, 22].

The Butler model considers the surface phase as an additional thermodynamic phase that is in equilibrium with the bulk. The interface between a bulk liquid solution and its equilibrium vapour as a surface phase is hypothesized to be monolayer [23]. Based on this, the surface tension of multicomponent liquid alloys, can be calculated by:

$$\sigma = \sigma_i + \frac{RT}{S_i} \ln \frac{X_i^s}{X_i^b} + \frac{1}{S_i} \{G_i^{xs,s}(T, X_j^s) - G_i^{xs,b}(T, X_j^b)\}, \quad (1)$$

$$i, j = 1, 2, 3 \dots$$

where X_j^k denotes an alloy composition with the subscript j and superscript k refer to the corresponding component j in the bulk, b and the surface phase, s . $G_i^{xs,b}(T, X_{j(j=2,3)}^b)$ and $G_i^{xs,s}(T, X_{j(j=2,3)}^s)$ are partial excess Gibbs energies of component i in the bulk phase and the surface phase, respectively, both as functions of temperature and composition. R , T , σ_p , S_i are gas constant, temperature, surface tension of pure component i , and surface area of component i , respectively. The Gibbs excess energy terms of binary and ternary alloys are given in the form of Redlich-Kister polynomials [24].

5. Results and discussion

5.1 Thermodynamics

No ternary compounds were detected in the Ag-Ge-Zn alloys. Table 3 summarizes the EDS global composition of the DSC samples together with the effects observed during heating. The primary phase which was formed upon solidification is also indicated. An undercooling of about 10 °C was generally observed. The invariant (i) and monovariant (m) temperatures were determined from the onset of the thermal effects during the heating step, and for the



liquidus temperature (l) the top of the peak was considered. As an example, Fig. 1 shows the heating and cooling curves for sample #16, in which four effects were identified. On heating, the P_1 invariant reaction at 282 °C, followed by the invariant U_2 at 590 °C, by the monovariant at 597 °C and finally the liquidus at 672 °C were determined.

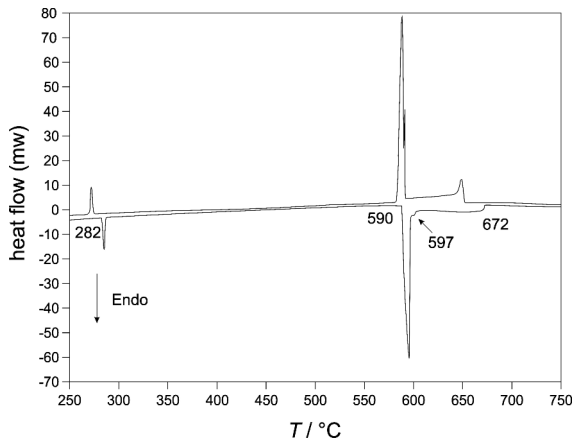


Figure 1. DSC heating and cooling curves (0.5 °C/min) of the Ag-Ge-Zn sample #16 (Ag36.5Ge24.5Zn39.0 at.%).

In several samples, a signal which could be related to the change of solubility of (Ag) as a function of temperature was observed on heating. For instance, sample #8 shows this endothermic effect between 530 and 575 °C, and sample #5 between 550 and 590 °C. Similarly, in the DSC curves of samples #10 (between 490 and 510 °C) and #12 (between 532 and 542 °C), effects related to the change of solubility of the β phase were observed. It can be underlined that the size of the effects associated to the change of the β phase solubility are smaller in comparison with those measured for the (Ag) phase.

On the basis of the experimental investigations, four invariant reactions ($U_1 - U_4$) involving the liquid phase were identified and two additional solid transition reactions (P_1 and U_5) were detected. The compositions of the participating liquid phases are shown in the proposed liquidus projection in Fig. 2. The invariant reactions are listed in Table 4 and the temperatures reported are averaged on the basis of the experimental results.

It should be underlined the presence of a wide (Ge) primary field in which the germanium shows Ag solubility lower than 1 at.% and a maximum solubility of Zn up to about 3 at.%.

The solubility of Ge in ζ and ε phases was found to be negligible, and a maximum value of 0.5 at.% was determined for the γ phase, see Table 5.

A reaction scheme consistent with our experimental observations is proposed in the Scheil diagram shown in

Table 4. Invariant reactions in the Ag-Ge-Zn ternary system, this work.

Reaction	Type	T/ °C
$L + (Ag) \rightleftharpoons \beta + (Ge)$	U_1	601
$L + \beta \rightleftharpoons \gamma + (Ge)$	U_2	591
$L + \gamma \rightleftharpoons \varepsilon + (Ge)$	U_3	570
$L + \varepsilon \rightleftharpoons (Ge) + (Zn)$	U_4	400
$\beta + \gamma + (Ge) \rightleftharpoons \zeta$	P_1	281
$\beta + (Ge) \rightleftharpoons (Ag) + \zeta$	U_5	263

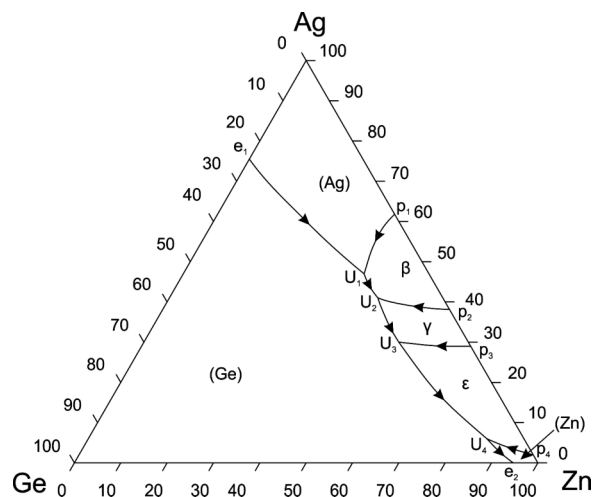


Figure 2. Ag-Ge-Zn system. Projection of the liquidus surface. Fields of primary crystallization are indicated; axes in at. %.

Fig. 3. The importance of the reaction scheme for the description of ternary and higher components systems have been highlighted in different papers [25, 26].

Because the samples were subjected to DSC measurements using slow heating and cooling rates (0.5 - 0.3 °C/min), a near equilibrium cooling process can be expected, and their final conditions were considered for the isothermal section at room temperature. The composition of the phases identified in these samples by SEM-EDS are listed in Table 5. Similar results were obtained for the annealed samples.

Fig. 4 shows the Ag-Ge-Zn isothermal section at room temperature. Four ternary phase fields have been determined: $(Ag) + \zeta + (Ge)$, $\zeta + \gamma + (Ge)$, $\gamma + \varepsilon + (Ge)$ and $\varepsilon + (Ge) + (Zn)$.

The vertex of the three phase fields is generally located at around 3 at.% Zn and at a content of Ag lower than the accuracy of the EDS probe. (Ag) and (Ge) form a wide two-phase field. Silver solves a maximum of Ge up to 6 at.%; for higher Zn content, the solubility of Ge in Ag considerably decreases (see e.g. samples #10 and #15).

Selected microphotographs Backscattered signal (BSE) of the analyzed alloys are reported in Figures 5-7.

Table 5. Summary of the phase compositions measured by SEM/EDS in the Ag-Ge-Zn ternary alloys at room temperature.

	SEM/EDS Composition (at.%)			Phase identified	Microstructure
	Ag	Ge	Zn		
1	82.9	5.8	11.3	(Ag)	Primary crystals of (Ag) surrounded by a fine eutectic-like mixture of (Ag)+(Ge)
	1.3	97.5	1.2	(Ge)	
2	81.8	5.9	12.4	(Ag)	Primary crystals of (Ag) surrounded by a fine eutectic-like mixture of (Ag)+(Ge)
	64.7	24.7	10.6	Mixture (Ag) + (Ge)	
3	82	6	12	(Ag)	Primary crystals of (Ag) surrounded by a fine eutectic-like mixture of (Ag)+(Ge), see Fig. 5
	1.2	97.8	1	(Ge)	
4	-	99.7	0.3	(Ge)	Few equiaxed (Ge) crystals and eutectic-like mixture of (Ag)+(Ge)
	79.2	3.7	17.1	(Ag)	
5	67.3	1.7	31	(Ag)	Primary crystals of (Ag) and eutectic-like mixture of (Ag) + (Ge)
	1.5	97.5	1	(Ge)	
	56.9	18.5	24.6	Mixture (Ag) + (Ge)	
6	70.5	2	27.5	(Ag)	Primary crystals of (Ag) and mixture of (Ag) + (Ge)
	1.6	97.9	0.5	(Ge)	
7	68.5	2.3	29.2	(Ag)	Primary crystals of (Ag) and mixture of (Ag) + (Ge)
	-	98	2	(Ge)	
8	66	1	33	(Ag)	Primary crystal of (Ag) and eutectic-like mixture of (Ag)+(Ge)
	-	98	2	(Ge)	
9	-	98.5	1.5	(Ge)	Primary big faceted crystals of (Ge) surrounded by a mixture of (Ag) and (Ge)
	76	4	20	(Ag)	
10	63	1	36	(Ag)	Three-phase sample: crystals of (Ge) in a matrix formed by (Ag) and ζ phases
	-	97.5	2.5	(Ge)	
	54	-	46	ζ	
11	72.5	2.5	25	(Ag)	Primary big faceted crystals of (Ge) surrounded by a mixture of (Ag) and (Ge)
	-	97.5	2.5	(Ge)	
12	-	3	97	(Ge)	Mixture of (Ge) and ζ phases and few small crystals of (Ag), see Fig. 6
	54	-	46	ζ	
13	49.6	-	51.4	ζ	Three-phase sample: needle and round-shaped crystals of (Ge) in a matrix of ζ and few γ phases
	40.5	0.5	59	γ	
	-	97	3	(Ge)	
14	-	97	3	(Ge)	Primary big faceted crystals of (Ge) surrounded by a mixture of ζ and (Ge) phases
	50	-	50	ζ	
15	-	97.5	2.5	(Ge)	Primary big faceted crystals of (Ge) surrounded by a mixture of (Ge) + (Ag) + ζ
	63	1	36	(Ag)	
	54	-	46	ζ	
16	-	97.2	2.8	(Ge)	Primary faceted (Ge) crystals in a matrix of ζ , γ and (Ge), see Fig.7.
	49.5	-	50.5	ζ	
	40.5	0.5	59	γ	
17	40.5	0.5	59	γ	Primary crystal of γ , crystals of (Ge) and ζ phase
	-	97.5	2.5	(Ge)	
	49.5	-	50.5	ζ	
18	37.5	-	62.5	γ	Three-phase sample: primary γ , (Ge) and few islands of ϵ phase.
	-	97	3	(Ge)	
	34	-	66	ϵ	
19	30	-	70	ϵ	Two-phase sample: few primary crystals of ϵ phase and mixture of (Ge) and ϵ phases.
	-	97	3	(Ge)	
20	13	-	87	ϵ	Primary ϵ crystals in a matrix of eutectic-like mixture of (Zn) and (Ge)
	4.5	-	95.5	(Zn)	
	-	97	3	(Ge)	

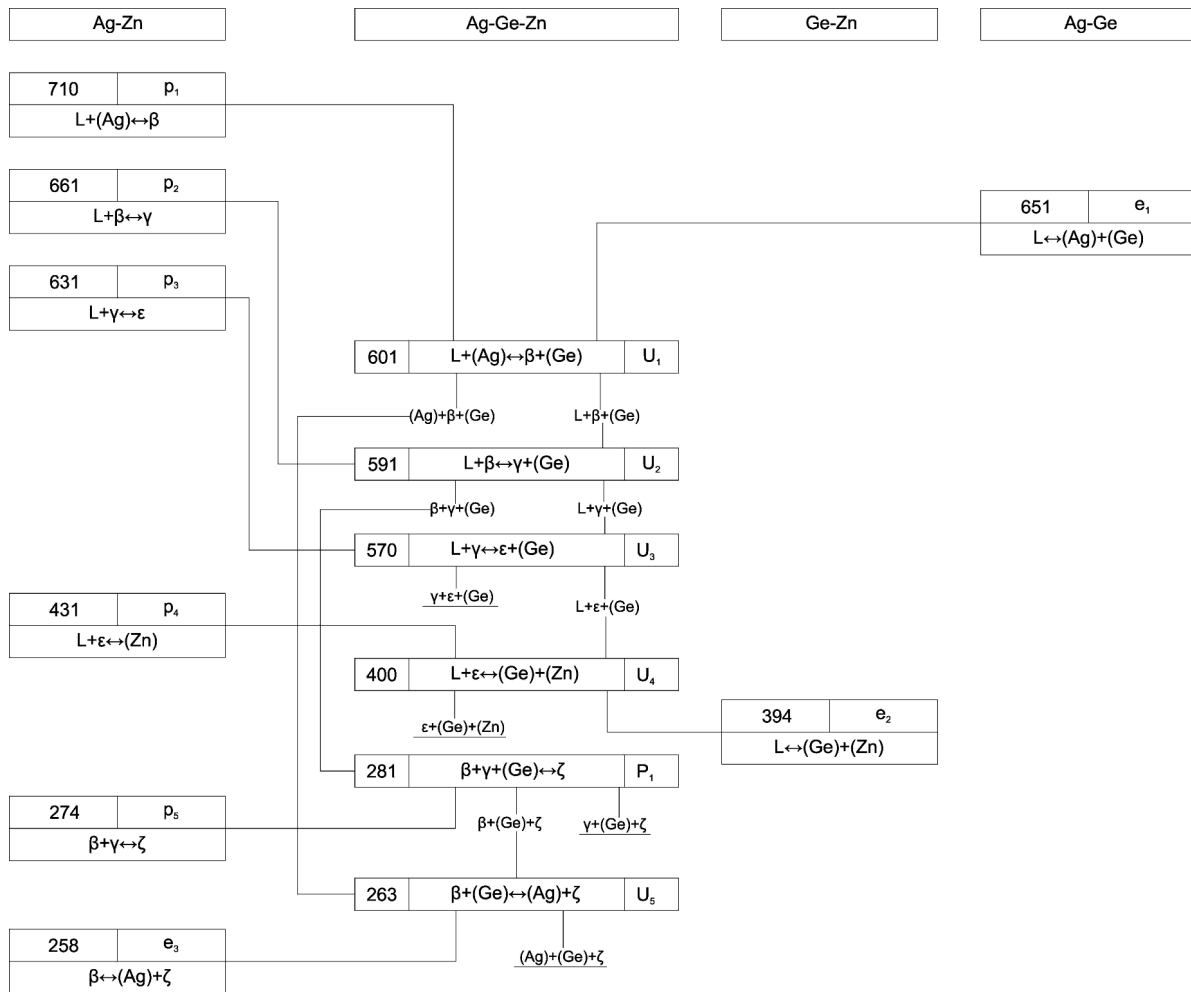


Figure 3. Reaction scheme in the Ag-Ge-Zn system.

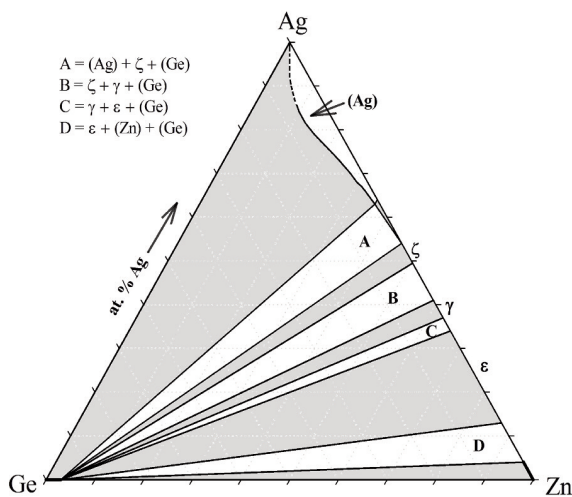


Figure 4. Ag-Ge-Zn system. Isothermal section at room temperature based on the results of the EDS analysis. The two phase fields are shaded in grey; axes in at.%.

Fig. 5 shows the micrograph of sample #3 with primary bright crystals of (Ag) surrounded by an eutectic-like mixture of (Ag) + (Ge). Fig. 6 shows the three-phase sample #12: black elongated (Ge) crystals, dark-grey ζ phase and few light-grey crystals of the (Ag) phase. Fig. 7 displays the micrograph of sample #16, with black (Ge) faceted primary crystals located at the border of the ingot, light-grey matrix made of γ and dark-grey of ζ phase.

5.2 Surface properties

The surface tension for Ag-Ge-Zn, Ag-Ge, Ag-Zn and Ge-Zn liquid alloys has been calculated using the Butler thermodynamic model in the regular solution approximation (Eq.(1)). The excess Gibbs energy terms of the Ag-Ge [16], Ag-Zn [10], and Ge-Zn [14] liquid binary phases were combined to describe the Gibbs free energy of Ag-Ge-Zn ternary melts. The reference data for the pure components, such as the surface tension of liquid Ag [5], Ge [5], Zn [27] and the molar volumes [28]



together with the Gibbs free energies of the binary liquid phases were used as input data for the calculations of the surface tension of ternary alloy melts. The isotherms of binaries and iso-surface tension lines of ternary alloys were calculated for 1000 °C. The surface tension isotherm of liquid Ag-Ge alloys was compared with two experimental datasets [4,5]. The experimental data of Ge-rich alloys [4] agrees fairly well with the

corresponding model predicted values, while the datasets [5] are closer to the surface tension isotherm, exhibiting differences in surface tension up to 10 % (Fig. 8a). The calculated surface tension isotherms for Ag-Zn and Ge-Zn alloys are reported in Figs. 8b and 8c, respectively, while the iso-surface tension lines for Ag-Ge-Zn alloys are shown in Fig. 9. Due to the lack of experimental data it was not possible to make a comparison between the theoretical and experimental data.

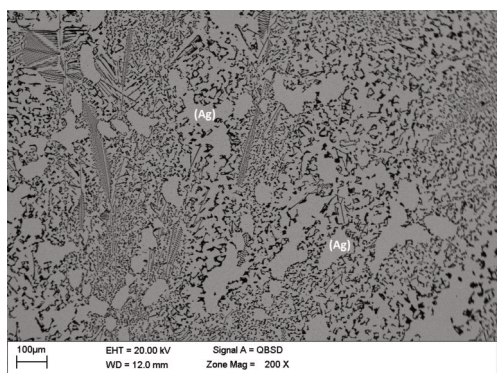


Figure 5. Backscattered electron (BSE) micrograph of the Ag-Ge-Zn Alloy #3 (Ag70.0Ge20.0Zn10.0 at.%): bright white phase (Ag), black phase (Ge).

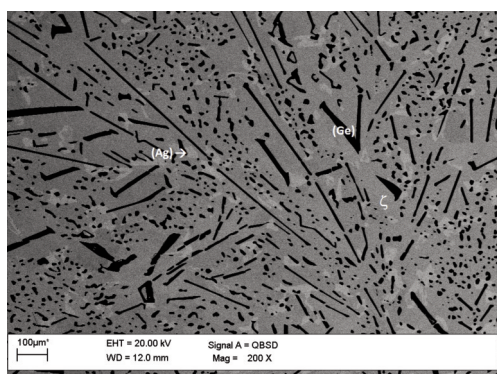


Figure 6. Micrograph (BSE signal) of Ag-Ge-Zn sample #12 (Ag47.0Ge15.5Zn37.5 at.%): black phase (Ge), dark-grey ζ phase, light-grey (Ag) phase.

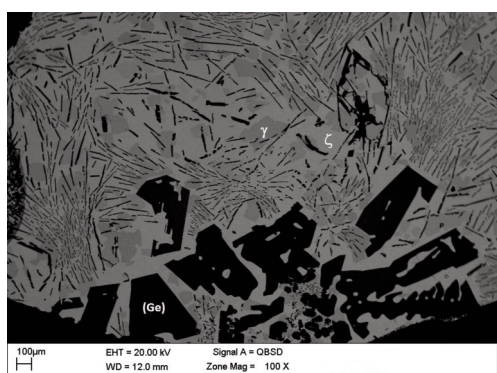


Figure 7. Micrograph (BSE signal) of Ag-Ge-Zn sample #16 (Ag36.5Ge24.5Zn39.0 at.%): black phase (Ge), dark-grey γ phase, light-grey ζ phase.

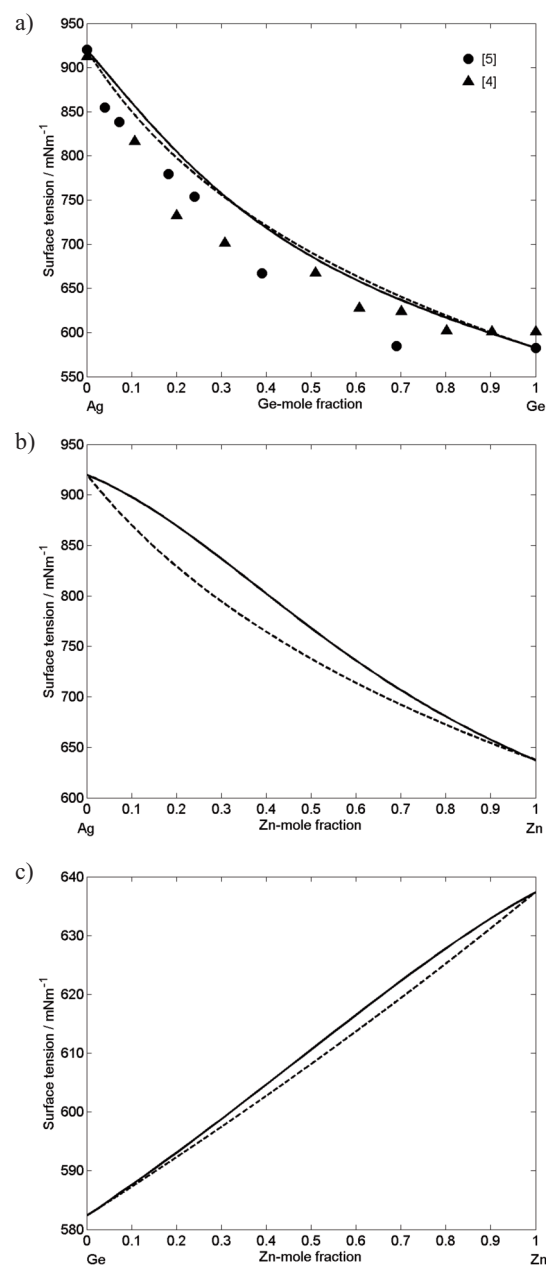


Figure 8. Surface tension isotherms for Ag-Ge (a), Ag-Zn (b) and Ge-Zn (c) liquid alloys at $T= 1000$ °C compared with literature data: line – calculation, symbols – experimental data [4,5]; ----- perfect solution model.

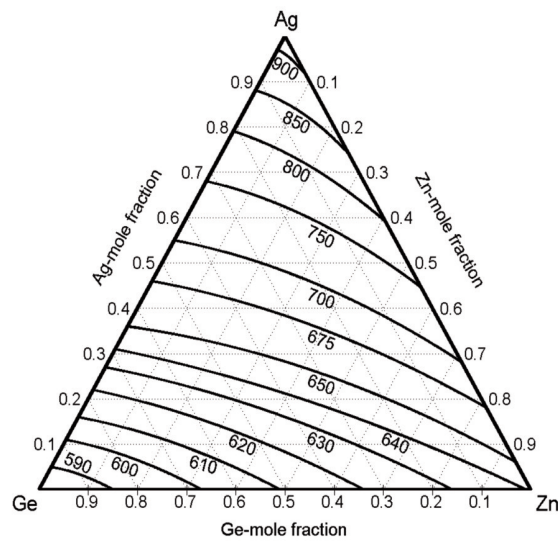


Figure 9. Iso-surface tension [mNm^{-1}] line for liquid Ag-Ge-Zn alloys calculated by using the Butler model for $T = 1000^\circ\text{C}$.

6. Conclusions

The knowledge of the phase equilibria and of the thermophysical properties of the Ag-Ge-Zn alloys can give basic information for industrial soldering process. A consistent description of the phase equilibria and of invariant reactions in the Ag-Ge-Zn ternary system has been described in the present work.

The liquidus projection and the corresponding reaction scheme have been proposed on the basis of the results obtained using different well-concerted techniques. The three components do not form any ternary phase and six invariant reactions are present. The isothermal section at room temperature shows four three-phase fields; the presence of Ag seems to promote the solubility of Zn in Ge up to 3 at. %.

Taking into account the importance of surface properties for joining processes, the model used to predict the surface tension values of the aforementioned alloy systems can be useful for the design of new braze/solder alloys.

References

- [1] J. R. Davis, K. Ferjutz, N.D. Wheaton, M.S. Woods (Eds.), *Welding, Brazing and Soldering*, Vol.6, ASM International, Materials Park, Ohio, USA, 1993, p. 114-125.
- [2] M. R. Pinasco, G. Pellati, A. Saccone, G. Borzone, E. Ricci, R. Novakovic, A. Passerone "Leghe a base di argento e procedimenti per la loro realizzazione, particolarmente per la fabbricazione di gioielli" Patent N. GE2006A000118, 2006.
- [3] S.W. Chen, J.C. Wang, L.C. Chen, *Intermetallics*, 83 (2017) 55-63.
- [4] N.A. Vatolin, V.F. Ukhov, V.P. Chenisov, *Akad. Nauk SSSR, Ural. Nauchn. Tsentr, Tr. Inst. Metall.*, 27 (1972) 86-91 (in Russian).
- [5] M. Brunet, J.C. Joud, N. Eustathopoulos, P. Desré, *J. Less-Common Met*, 51 (1977) 69-77 (in French).
- [6] Y. Plevachuk, V. Sklyarchuk, G. Gerbeth, S. Eckert, R. Novakovic, *Surf. Sci.*, 605(11-12) (2011) 1034-1042.
- [7] V. Sklyarchuk, Yu. Plevachuk, I. Kaban, R. Novakovic, *J. Min. Metall. Sect. B-Metall.*, 48 (3) B (2012) 443-448.
- [8] K.W. Andrews, H.E. Davies, W. Hume-Rothery, C.R. Oswin, *Proc. Roy. Soc. (London)*, A177 (1941) 149-167.
- [9] T.B. Massalski, H. Okamoto, P.R. Subramanian, L. Kacprzak (Eds.), *Binary Alloy Phase Diagrams*, 2nd Edition., Vols. 1-2, ASM International, Materials Park, Ohio, USA, 1990, p. 39-42, 117-118, 2023-2026.
- [10] T. Gomez-Acebo, *Calphad*, 22(2) (1998) 203-220.
- [11] V.T. Witusiewicz, S.G. Fries, U. Hecht, A. Drevermann, S. Rex, *Int. J. Mater. Res. (formerly Z. Metallkd.)*, 97 (5) (2006) 556-568.
- [12] D. Zivkovic, D. Manasijevic, D. Minic, L.J. Balanovic, M. Premovic, A. Kostov, A. Mitovski, *J. Chem. Technol. Metall.*, 48(4) (2013) 413-418.
- [13] P. Villars, K. Cenzual, *Pearson's Crystal Data - Crystal Structure Database for Inorganic Compounds (on DVD)*, Release 2016/17, ASM International, Materials Park, Ohio, USA.
- [14] P.-Y. Chevalier, *Thermochim. Acta*, 130 (1988) 25-32.
- [15] R.W. Olesinski, G.J. Abbaschian, *Bulletin of Alloy Phase Diagrams*, 9(1) (1988) 58-64.
- [16] J. Wang, Y.J. Liu, C.Y. Tang, L.B. Liu, H.Y. Zhou, Z.P. Jin, *Thermochim. Acta* 512 (2011) 240-246.
- [17] R. Manaila, F. Zavaliche, R. Popescu, D. Macovei, A. Devenyi, C. Bunescu, E. Vasile, A. Jianu, *Mater. Sc. Eng.*, A226-228 (1997) 290-295.
- [18] R.W. Olesinski, G.J. Abbaschian, *Bulletin of Alloy Phase Diagrams*, 6(6) (1985) 540-543.
- [19] I. Egry, E. Ricci, R. Novakovic, S. Ozawa, *Advances in Colloid and Interface Science*, 159 (2010) 198-212.
- [20] J. Lee, W. Shimoda, T. Tanaka, *Mater. Trans.*, 45 (2004) 2864-2870.
- [21] Z. Moser, W. Gąsior, J. Pstruś, S. Ishihara, X.J. Liu, I. Ohnuma, R. Kainuma, K. Ishida, *Mater. Trans.*, 45(3) (2004) 652-660.
- [22] C. Costa, S. Delsante, G. Borzone, D. Zivkovic, R. Novakovic, *J. Chem. Thermodynamics*, 69 (2014) 73-84.
- [23] J.A.V. Butler, *Proc. Roy. Soc. A* 135 (1932) 348-375.
- [24] N. Saunders, A.P. Miodownik, *CALPHAD (Calculation of Phase Diagrams): A Comprehensive Guide*, Pergamon, Exeter, 1998.
- [25] H.L. Lukas, E.-T. Henig, G. Petzow, *Z. Metallkd.*, 77 (1986) 360-367.
- [26] J. Zhao, J. Zhou, S. Liu, Y. Du, S. Tang, Y. Yang, *J. Min. Metall. Sect. B-Metall.*, 52 (1) B (2016) 99-112.
- [27] V.A. Paramanov, E.F. Karamyshev, V.F. Ukhov, *Fiz. khim. poverkh. rasp.*, Tbilisi, (1955) p.155.
- [28] T. Iida, R.I.L. Guthrie, *The physical properties of liquid metals*, 1st edn. Clarendon Press, Oxford, 1993, p.124.

